UC Irvine
UC Irvine Previously Published Works

Title

Potent and Selective Human Neuronal Nitric Oxide Synthase Inhibition by Optimization of the 2-Aminopyridine-Based Scaffold with a Pyridine Linker

Permalink

https://escholarship.org/uc/item/00m4m3f7

Journal

Journal of Medicinal Chemistry, 59(10)

ISSN

0022-2623

Authors

Wang, Heng-Yen
Qin, Yajuan
Li, Huiying
et al.

Publication Date

2016-05-26

DOI

10.1021/acs.jmedchem.6b00273

Copyright Information

Peer reviewed

Potent and Selective Human Neuronal Nitric Oxide Synthase Inhibition by Optimization of the 2-Aminopyridine-based Scaffold with a Pyridine Linker

Heng-Yen Wang[†,¥], **Yajuan Qin**[†,‡,¥], **Huiying Li**[§], **Linda J. Roman**[¶], **Pavel Martásek**[¶,£,#], **Thomas L. Poulos**[§,*], and **Richard B. Silverman**[†,*]

[†]Department of Chemistry, Department of Molecular Biosciences, Chemistry of Life Processes Institute, Center for Molecular Innovation and Drug Discovery, Northwestern University, 2145 Sheridan Road, Evanston, Illinois 60208-3113, United States

[‡]State Key Laboratory of Pharmaceutical Biotechnology, School of Life Sciences, Nanjing University, Nanjing 210093, People's Republic of China

[§]Departments of Molecular Biology and Biochemistry, Pharmaceutical Sciences, and Chemistry, University of California, Irvine, California 92697-3900, United States

[¶]Department of Biochemistry, University of Texas Health Science Center, San Antonio, Texas 78384-7760, United States

[£]Department of Pediatrics, First Faculty of Medicine, Charles University, Prague, Czech Republic

[#]BIOCEV, Prague, Czech Republic

Abstract

Neuronal nitric oxide synthase (nNOS) is an important therapeutic target for the treatment of various neurodegenerative disorders. A major challenge in the design of nNOS inhibitors focuses on potency in humans and selectivity over other NOS isoforms. Here we report potent and selective human nNOS inhibitors based on the 2-aminopyridine scaffold with a central pyridine linker. Compound **14j**, the most promising inhibitor in this study, exhibits excellent potency for rat nNOS (K_i 16 nM) with 828-fold n/e and 118-fold n/i, selectivity, with a K_i value of 13 nM against human nNOS with 1761-fold human n/e selectivity. Compound **14j** also displayed good metabolic

[*]Corresponding Authors: (T.L.P.) Tel:+1 949 824 7020. ; Email: poulos@uci.edu. (R.B.S.) Tel:+1 847 491 5653. Fax: +1 847 491 7713. ; Email: Agman@chem.northwestern.edu

[¥]These author contributed equally.

Notes

The authors declare no competing financial interest.

stability in human liver microsomes, low plasma protein binding, and minimal binding to cytochromes P450 (CYPs), although it had little to no Caco-2 permeability.

Graphical abstract
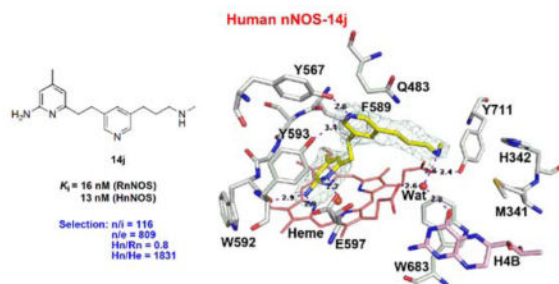
Keywords

nitric oxide synthase; neurodegenerative diseases; mutant nNOS; human nNOS; human eNOS; selective inhibition

Introduction

Nitric oxide (NO) is an essential second messenger in mammals,[1] which regulates a variety of biological processes, such as vasodilation,[2] smooth muscle relaxation,[3] neurotransmission,[4] and immune response.[5] NO is generated by nitric oxide synthases (NOSs), of which there are three mammalian NOS isoforms: inducible NOS (iNOS), which activates the immune system to destroy pathogens and microorganisms;[6] endothelial NOS (eNOS), which regulates the relaxation of smooth muscle, leading to a decrease of blood pressure;[7] and neuronal NOS (nNOS), which regulates the release of neurotransmitters[8] and is involved in neuronal communication.[9] Overproduction of NO in the central nervous system (CNS) has been reported to be associated with chronic neurodegenerative pathogenesis,[10] such as Alzheimer's disease (AD),[11] Parkinson's disease (PD),[12] and Huntington's disease (HD),[13] as well as amyotrophic lateral sclerosis (ALS).[14] Therefore, inhibition of nNOS is a viable therapeutic strategy for treating neurodegenerative disorders.

All of the mammalian NOSs are active only as homodimers,[15] and each monomer consists of a C-terminal reductase domain, which contains the binding sites for NADPH (reduced nicotinamide adenine dinucleotide phosphate), FAD (flavin adenine dinucleotide), and FMN (flavin mononucleotide),[16] and an N-terminal oxygenase domain, which contains binding sites for non-catalytic zinc (Zn^{2+}), catalytic heme, cofactor H_4B (tetrahydrobiopterin), and the substrate(L-Arg).[17] NOSs catalyze the oxidation of L-Arg to L-citrulline and NO in the presence of oxygen and NADPH, and this cascade reaction is initiated by the two-electron donor NADPH in the reductase domain to the electron acceptor heme in the oxygenase domain through FAD and FMN with a series of proton transfers in the process.[18]

Given that all NOS isoforms catalyze the same reaction, the active site structures are nearly identical, which has made the development of isoform-selective inhibitors a challenging

problem. Nevertheless, it has been possible to exploit subtle difference in the active sites to develop highly selective nNOS inhibitors.[19] Current efforts have been focused on improving bioavailability without sacrificing potency and selectivity. Various nNOS inhibitors that we have developed are shown in Figure 1. Thiophene-based inhibitors with diamine and hydroxyethyl-diamine structure (Figure 1, **1** and **2**, respectively)[20] show good potency against human nNOS. However, compound **2** gives very poor isoform selectivity over iNOS and eNOS (n/I = 49 and n/e = 48). Compound **3**,[21,22] containing 2-aminopyridine, a pyrrolidine linker, and a diamine tail, is a moderate nNOS inhibitor (K_i = 388 nM) with good isoform selectivity (1114-fold over bovine eNOS and 150-fold over murine iNOS). Compound **4**,[23] a double-headed inhibitor, displays good potency against nNOS (K_i= 25 nM) but lacks good isoform selectivity (n/e=107 and n/i=58). Recently, our group reported a series of nNOS inhibitors with a 2-aminopyridine anchor, a heteroaromatic ring linker, and a diamine tail, such as compounds **5** and **6**.[24] Both display excellent potency for rat nNOS (K_i=17 nM and 35 nM, respectively) and good selectivity over iNOS and eNOS (**5**: n/i= 127, n/e= 759; **6**: n/i= 138, n/e=507). However, compounds **5** and **6** exhibit decreased potency against human nNOS (59 nM and 64 nM, respectively).

Although the human NOS isoforms are the ultimate target for these inhibitors, our efforts have focused on rat nNOS and bovine eNOS[25–30] primarily because these two NOS isoforms generate the best crystals. However, we recently have been able to crystallize human nNOS and eNOS and have found that potencies for our inhibitors were generally 5–10 times less with human nNOS than with rat nNOS. This could be a problem for translation of preclinical animal studies to clinical trials, and could, in general, account for some drug failures in clinical trials. An overlay of human and rat nNOS crystal structures showed that the primary sequence in the active site and peripheral pocket of the rat enzyme is almost identical to that in the human enzyme except that Leu337 in the rat nNOS peripheral pocket is replaced by His342 in human nNOS. Consequently, the peripheral pocket of human nNOS tends to bind smaller and more hydrophilic inhibitors, providing an insightful guide for the design of more potent human nNOS inhibitors.[24, 29b]

On the basis of reported NOS assay results and X-ray crystallographic analysis, we performed specific and structure-based optimizations to improve the potency and selectivity of lead **5**. Major modifications focused on exploring the diversity of the tail portion, leaving the aminopyridine head and middle pyridine linker unmodified. First, we adopted a ring-chain transformation strategy to give compound **14b**, based on the structure of **14a**, to investigate the influence of a bulker and more hydrophobic tail on the potency and selectivity of nNOS inhibitors. Second, an O atom and N atom were employed as bioisosteric replacements in the piperidine ring of **14b** to make **14c** and **14g**, where the O atom or N atom could possibly make a direct or indirect (water-assisted) H-bond network with the heme, H_4B, or the surrounding residues within the active site of nNOS. Next, a ring-chain transformation and homologation were used to design **14d** and **14e** from**14c**, and the piperazine tail of **14g** was bioisosterically changed to a piperidine ring to obtain **14h**. Lastly, **14j** and **14k**were synthesized, adopting a ring-chain transformation strategy from **14h** to investigate the influence of flexibility on activity. The SAR of the secondary and tertiary amines on the tail were explored to evaluate steric and polar effects.

All compounds were assayed against purified rat nNOS, murine iNOS, and bovine eNOS for preliminary evaluation of the potency and isoform selectivity for the NOSs in lower animals. Many of the compounds were also assayed against human nNOS and eNOS to determine human isoform selectivity.

CHEMISTRY

The synthesis of compounds **10** and **11** is shown in Scheme 1. Compound **11** was prepared in two steps, coupling 3-chloromethylpyridine (**8a**) with lithiated pyrrolyl-4,6-dimethylpyridine (**7**) followed by pyrrole deprotection.[24] Intermediate **10** was synthesized by the same coupling reaction described above using aryl bromide **8b**.

As shown in Scheme 2, compounds **14a-14e** were synthesized by palladium-catalyzed Buchwald-Hartwig amination of intermediate **10** with amines **12a-12e**[24,31] followed by pyrrole deprotection.[24] Compound **10** was subjected to palladium-catalyzed amination with **12f** to give **13f**, which was methylated (**13g**), and the pyrrole was deprotected to afford **14g**.

The synthesis of **14h** is shown in Scheme 3. Compound **13h** was obtained via Suzuki cross-coupling[32] employing **10** and boronic acid **12h; 13h** subsequently underwent alkene reduction, carbamate reduction, and pyrrole deprotection to give **14h**. Compound **14j** and **14k** were synthesized according to Scheme 4. Compound **14j** was prepared in three steps including a Sonagashira cross-coupling[33] of **10** with *N*-Boc-*N*-methyl-propargylamine (**12i**), Boc deprotection, and pyrrole deprotection. Sonagashiracross-coupling of **10** with 3-dimethylamino-1-propyne (**12k**) followed by pyrrole deprotection gave **14k**.

RESULTS AND DISCUSSION

Inhibition of nonhuman NOSs

Synthesized inhibitors were assayed against purified rat nNOS, murine macrophage iNOS, bovine eNOS, and human nNOS and eNOS using the hemoglobin capture assay.[34,35] The K_i values and isoform selectivities for inhibitors **11**, **14a-14e**, **14g**, **14h**, **14j**, and **14k** against nonhuman NOSs are shown in Table 1; values for **4**,[23] **5**,[24] and **6**[24] are included for comparison. The excision of the terminal pyridino or amino group from **4-6** is highly detrimental to the potency (see **11**-**14e**). Addition of a second amino group by attachment of a piperazine (**14g**) or piperidine (**14h**) ring begins to restore the excellent potencies and selectivities of **4-6**. The crystal structures of nNOS-**14g** (Figure 4A) and nNOS-**5** (Figure 4C) reveal a similar and unique inhibitor binding mode. In addition to the 2-aminopyridine-Glu592 H-bond, the pyridine linker bends upward forming a H-bond to Tyr562 (3.0 Å). To allow this upward pyridine position the Gln478 side chain has to adapt to an alternate rotamer form. The external N atom in the piperazine ring joins a H-bonding network involving H$_4$B and heme propionate A *via* a water molecule (external N to water: 3.0 Å; water to H$_4$B: 2.7 Å; water to heme propionate A: 2.6 Å). In contrast, for **5**, although the internal N atom position in the tail is well-defined, the positions of the last three atoms are ambiguous, having weaker density.[24]

The internal N atom in the tail region attached to the pyridine linker does not interact with the surrounding residues, as shown in both the nNOS-**14g** and nNOS-**5** complexes. On the basis of the crystal structures, **14h** was synthesized as a bioisostere of **14g** without the internal N atom in the piperazine ring. As shown in the crystal structure of nNOS-**14h** (Figure 4B), in addition to the strong 2-aminopyridine-Glu592 salt bridge, the N atom in the pyridine linker forms a H-bond to Tyr562 (3.0 Å), and the N atom in the piperazine ring also participates in a water-assisted H-bonding network with the H_4B and heme propionate A (N atom to water: 2.9 Å; water to H_4B: 2.6 Å; water to heme propionate A: 2.7 Å). Therefore, **14g**, **14h**, and **5** bind identically to rat nNOS with the pyridine linker in an upward position, i.e., in which the pyridine N faces away from the heme. The differences in potency among **14g**, **14h,** and **5** could be explained by the flexibility of the tail region and the strength (H-bond distance) of the interaction made by the central pyridine linker to Tyr562.

Compound **14g** is a very weak inhibitor of bovine eNOS (K_i>30000 nM), at least 2.5-fold less potent than reference compound **5** (K_i 12910 nM); consequently, it is highly selective for nNOS over eNOS (n/e > 698). The crystal structure of eNOS-**14g** (Figure 6A) shows that while the 2-aminopyridine forms H-bonds with Glu363, the pyridine linker is no longer in the upward position. Rather, it forms a H-bonding network involving the H_4B and heme propionate A *via* a water molecule (N atom to water: 2.7 Å; water to H_4B: 2.6 Å; water to heme propionate A: 2.5 Å), and the external N atom in the piperazine ring forms a weak H-bond with Asn340 (3.4 Å). In comparison, the central pyridine linker in the eNOS-**5** complex (Figure 6B) is also in a flat binding mode, and the tail region of **5** does not interact with the enzyme. The pyridine linker in **14g** is parallel to the 2-aminopyridine anchor, while the pyridine linker in **5** makes a 15° angle from the 2-aminopyridine plane, which does not involve the H-bonding network with H_4B and heme. The excellent n/e selectivities for **14g** and **5** are very likely the result of the drastically different pyridine linker positions in the two isoforms.

The most potent and selective analogues (**14j** and **14k**) have flexible side chains resembling that in **5**, except that the *N*-methylamino group adjacent to the pyridine ring has been replaced by a methylene group. In a comparison of the crystal structures of nNOS-**14j** and nNOS-**14k** (Figure 6) with that of nNOS-**5** (Figure 4C), the 2-aminopyridine-Glu592 interaction and the identical upward pyridine linker binding mode are observed in all three of the complexes. In the nNOS-**14j** complex, the secondary amine N atom in the tail region joins a water-assisted H-bonding network with the H_4B and heme propionate A (N atom to water: 2.9 Å; water to H_4B: 2.6 Å; water to heme propionate A: 2.6 Å). In the **14k**-nNOS complex, the tertiary amine N atom in the tail region also participates in a water-bridged H-bonding network involving the H_4B and heme propionate A (N atom to water: 2.6 Å; water to H_4B: 2.6 Å; water to heme propionate A: 2.6 Å). The involvement of the inhibitor tail region with a H-bonding network seems to improve potency.

Consistent with the observed high n/e selectivity, the crystal structure of eNOS-**14k** (Figure 6C) shows that the upward pyridine linker binding mode of **14k** in nNOS is not observed in eNOS. Rather, its linker pyridine is parallel to the plane of the aminopyridine anchor, making H-bonds with Asn368 *via* a bridging water molecule (N atom to water: 2.9 Å; water

to Asn368: 2.9 Å). In addition, the tertiary amine N on the tail forms a H-bond with heme propionate D (2.9 Å).

Inhibition of human NOSs

The primary sequence of human and rat NOS is more than 93% identical,[24] and the nNOS active site in each mammalian isozyme is highly conserved. The peripheral pockets of human- and rat nNOS differ by only one residue (His342 in human and Leu337 in rat).[24, 36] If the inhibitor is designed so it is too small to reach the His342/Leu337 site, an identical binding mode should be observed in both the human and rat nNOS-inhibitor complexes,[24] and the difference in potency of an inhibitor for the enzyme in these species should be insignificant (K_i human nNOS/rat nNOS close to 1). Compounds **5** and **6** fit into this classification, and the human nNOS/rat nNOS ratios for these compounds were 3.5 and 1.8, respectively.

Compounds **14a**, **14c**, **14g**, **14h**, **14j**, and **14k**, which also have truncated side-chains, were assayed against purified human nNOS (Table 2). Four of these analogues, **14c**, **14h**, **14j**, **14k**, had human nNOS/rat nNOS ratios lower than 1.8; **14j** is the first potent compound with a human nNOS/rat nNOS ratio < 1. The benefit of a human/rat K_i ratio of 1 or less is that results in a preclinical rodent model might translate to humans in clinical trials.

As shown in Figure 7A, the 2-aminopyridine group of **14g** forms H-bonds with Glu597 in human nNOS (Glu592 in rat); the N atom in the pyridine linker makes a H-bond with Tyr567 (2.8 Å) (Tyr562 in rat); the external N atom in the piperazine ring joins a H-bond network involving H_4B and heme propionate A *via* a water molecule (external N to water: 2.9 Å; water to H_4B: 3.0 Å; water to heme propionate A: 2.5 Å). In the human nNOS-**14h** complex (Figure 7B), the same H-bonds exist between the 2-aminopyridine group of **14h** and Glu597; the N atom of the pyridine linker makes a H-bond to Tyr567 (3.0 Å), and the external N atom in the piperazine ring participates in a water-assisted H-bonding network involving H_4B and heme propionate A (external N to water: 2.7 Å; water to H_4B: 2.8 Å; water to heme propionate A: 2.7 Å).

The human nNOS-**14g** crystal structure (Figure 7A) shows an identical upward pyridine linker binding mode as shown in Figure 4A (rat nNOS-**14g**) because **14g** is too short to reach the His342/Leu337 site (His342 is at least 8 Å away from **14g**). Similarly, an identical binding mode is observed in both human and rat nNOS-**14h** complexes (Figure 7B and Figure 4B).

Compound **14j** is comparable in potency and selectivity to those of compound **5; 14k** has two-thirds the potency of **5** with lower selectivity. Crystal structures of these compounds bound to human nNOS show that **14j** (Figure 8A) H-bonds to Glu597 through the 2-aminopyridine group; the N atom in the pyridine linker forms two H-bonds to Tyr567 (2.8 Å) and Tyr593 (3.4 Å) (Tyr588 in rat), and the N atom in the tail region participates in a tight H-bonding network involving the H_4B and heme propionate A through a water molecule (N to water: 2.6 Å; water to H_4B: 2.8 Å; water to heme propionate A: 2.6 Å). Similar interactions are involved in the **14k** complex (Figure 8B). In addition to the 2-aminopyridine-Glu597 interaction, the N atom in the pyridine linker forms two H-bonds to

Tyr567 (2.8 Å) and Tyr593 (3.5 Å), and the N atom in the tail region joins a water-mediated H-bond network with H_4B and heme propionate A (N to water: 2.5 Å; water to H_4B: 2.9 Å; water to heme propionate A: 2.7 Å). The structures of human nNOS-**14j** and -**14k** reveal a subtle but important feature: the N atom in the pyridine linker is involved in two H-bonds; the distance to Tyr593 is within 3.5 Å. This is the consequence of a long tail region where its amine N atom is part of a tight H-bonding network with the H_4B and heme *via* a water molecule. The network pushes the pyridine linker closer to Tyr567 and Tyr593. This feature does not exist in structures of human nNOS-**14g** or -**14h** because the H-bonding network there is established by shorter piperidine or piperazine moieties. In all of the rat nNOS structures in complex with **14g**, **14h**, **14j**, and **14k**, the N atom in the pyridine linker is also only making one H-bond with Tyr562, but not with Tyr588. A comparison with the binding interactions in human nNOS-**5** (Figure 8C) is interesting as well. While the 2-aminopyridine group in **5** is also anchored by Glu597, the N atom of the central pyridine ring makes only one hydrogen bond, that is, with Tyr567, and the external N atom in the tail region displaces the bridging water molecule between the H_4B and heme propionate A.[24] All three inhibitors, **14j**, **14k**, and **5**, exhibit the same upward pyridine binding mode in human nNOS; the differences in the enzyme-inhibitor interactions, especially in the number and distances of the H bonds, appear to account for the compound potency differences.

An alignment of human nNOS and eNOS reveals four important residue differences: Ser607/His371, His342/Phe305, Met341/Val104, and Asp602/Asn366. Among these four amino acid pairs, the Asp602/Asn366 difference in human nNOS/eNOS makes the nNOS active site more electronegative than eNOS, and this electronic difference can be used for selective inhibition (nNOS tends to bind positively charged compounds).

Compounds **14a**, **14c**, **14g**, **14h**, **14j**, and **14k** were assayed against purified human eNOS and compared with **5** and **6** (Table 3). Once again, **14j** exhibited the best selectivity properties of these compounds, 1761-fold more potent against human nNOS than human eNOS. Although **14g** had the least affinity for human eNOS, its potency with human nNOS was 6.5 times worse than that for **14j**, so the selectivity of **14g** was about half that of **14j**.

Effect of 14j on CYPs

The two pyridines in **14j** make it a potential inhibitor of cytochromes P450 (CYPs). Consequently, **14j** was evaluated for its inhibition of seven major human liver microsomal P450s (Table 4). At a concentration 769 times its K_i against human nNOS (10 μM), it was found to inhibit the activity of CYP1A2, CYP2B6, CYP2C8, CYP2C9, CYP2C19, and CYP2D6 insignificantly; the only isozyme that showed any significant inhibition was CYP3A4 (58%). The IC_{50} of compound **14j** for CYP3A4 is estimated to be approximately 10 μM, and the selectivity toward nNOS is more than 70-fold in rat (IC_{50} 0.142 μM) and 100-fold in human (IC_{50} 0.091 μM). Therefore, the inhibitory potency of **14j** for CYP3A4 is relatively weak.

Other pharmacokinetic properties of 14j

Other pharmacokinetic properties that were tested with **14j** included human microsome stability and plasma protein binding. At 1 μM concentration, the half-life of **14j** in human

liver microsomes was > 60 min; however, the metabolism was unrelated to CYP-mediated metabolism, as 23% of the compound was lost in 60 min in the absence of NADPH or in 90 min in the presence of NADPH. At 5 μM concentration, only 20% bound to human plasma protein. Unfortunately, **14j** exhibited little or no Caco-2 permeability. Detailed experimental results and protocol can be found in the Supporting Information.

CONCLUSIONS

A series of human nNOS inhibitors, based on the 2-aminopyridine scaffold having a central pyridine linker, were designed and evaluated. Compound **14j** had outstanding properties, exhibiting a potent and slightly lower K_i value for human nNOS (13 nM) than rat nNOS (16 nM) with 118-fold and 1761-fold selectivity over mouse iNOS and human eNOS, respectively. X-ray crystal structures of **14j** bound to both rat and human nNOS showed that the N of the pyridine linker formed two H-bonds (to Tyr567 and Tyr593) in human nNOS but only one H-bond in rat nNOS. Compound **14j** displayed very poor inhibition of human CYPs (except 58% inhibition of CYP3A4 at 10 μM), little or no human microsome CYP metabolism for at least 60 min, and only 20% human plasma protein binding. However, it had little or no Caco-2 permeability, predicting that oral absorption would be poor.

EXPERIMENTAL SECTION

Materials, Synthetic Methods, and Characterization of Molecules

Commercially available starting materials **12a-12f** were purchased from Sigma-Aldrich and were used without further purification. All reactions were performed under an atmosphere of dry argon. Compounds **7**, **8a**, **8b**, **12h**, and **12i** were prepared by known literature procedures using commercially available chemicals (**7-s**, **8a-S**, **8b-S**, **12h-S**, and **12i-S;** see Supporting Information for details), and their spectral data are consistent with those data reported for them.

Anhydrous solvents (CH_2Cl_2 and THF) were purified prior to use by passage through a column composed of activated alumina and a supported copper redox catalyst. Analytical thin-layer chromatography was carried out on SiliCycle pre-coated silica gel 60 F254 plates. Compounds were visualized with short-wavelength UV light, ninhydrin, or $KMnO_4$ stain. Flash column chromatography was performed using an Agilent 971-FP automated flash purification system with a Varian column station and various SiliCycle cartridges (4–80 g, 40–63 μm, 60 Å). ^{1}H NMR and ^{13}C NMR spectra were recorded in the indicated solvent on a Bruker Avance-III (500 MHz and 125 MHz for ^{1}H and ^{13}C, respectively) spectrometer. Low-resolution ESIMS was performed using a Bruker AmaZon SL Ion Trap mass spectrometer system. High-resolution mass spectra were obtained using an Agilent 6210 LC-TOF spectrometer in the positive ion mode using electrospray ionization with an Agilent G1312A HPLC pump and an Agilent G1367B auto injector at the Integrated Molecular Structure Education and Research Center (IMSERC), Northwestern University. The purity of the compounds was evaluated on an analytical HPLC. Analytical HPLC was performed using an Agilent Infinity 1260 HPLC system with a Phenonemex Luna C-8 (4.6 × 250 mm, 5 μm) reverse phase column, detecting with UV absorbance (254 nm). The purity of all compounds that were subjected to biological assay was > 95%.

General Procedure A: Pyrrolyl-lutidine and Aryl Halide Coupling

A round bottom flask was charged with **7** (1 equiv.), and THF was added to form a 0.2 M solution. *n*-BuLi (1.6 equiv.) was added to the solution at −78 °C, and the reaction mixture was allowed to stir for 30 min at 0 °C. The mixture was transferred to a 1 M solution of aryl halide (**8a** or **8b**) in THF *via* cannula at −78 °C, which was allowed to stir for an additional 20 min then quenched with H_2O. The crude reaction mixture was partitioned between ethyl acetate and water, and the organic layer was washed with H_2O and brine, dried with Na_2SO_4, and concentrated under reduced pressure. The crude product was purified by flash column chromatography to give **9** and **10**.

2-(2,5-Dimethyl-1*H*-pyrrol-1-yl)-4-methyl-6-(2-(pyridin-3-yl)ethyl)pyridine (9)—
Compound **9** was synthesized according to general procedure **A** using **7** (600 mg, 3 mmol) and **8a** (681 mg, 3 mmol). **9** was isolated as a yellow oil (343 mg, 39%) after flash column chromatography (ethyl acetate: hexanes 1:1). ^1H NMR (500 MHz, CDCl$_3$): δ 8.41–8.39 (m, 2H), 7.46 (d, *J* = 5.0 Hz, 1H), 7.16 (dd, *J* = 7.0, 5.0 Hz, 1H), 6.87 (s, 1H), 6.84 (s, 1H), 5.86 (s, 2H), 3.06–3.05 (m, 4H), 2.33 (s, 3H), 2.09 (s, 6H); ^{13}C NMR (125 MHz, CDCl$_3$): δ 160.1, 151.8, 150.0, 149.6, 147.5, 136.7, 135.9, 128.5, 123.3, 122.7, 120.3, 106.8, 39.1, 32.7, 21.0, 13.2; MS ESI: calcd. For $C_{19}H_{22}N_3$ $[M+H]^+$, 292.18; found, 292.08.

2-(2-(5-Bromopyridin-3-yl)ethyl)-6-(2,5-dimethyl-1H-pyrrol-1-yl)-4-methylpyridine (10)—Compound **10** was synthesized according to general procedure **A** using **7** (400 mg, 2 mmol) and **8b** (500 mg, 2 mmol). **10** was isolated as a yellow oil (273.2 mg, 46%) after flash column chromatography (ethyl acetate: hexanes 1:4). ^1H NMR (500 MHz, CDCl$_3$): δ 8.48 (s, 1H), 8.30 (s, 1H), 7.60 (s, 1H), 6.87 (s, 1H), 6.86 (s, 1H), 5.87 (s, 2H), 3.06–3.05 (m, 4H), 2.35 (s, 3H), 2.09 (s, 6H); ^{13}C NMR (125 MHz, CDCl$_3$): δ 159.4, 151.9, 149.8, 148.2, 147.6, 139.1, 138.9, 128.5, 122.8, 120.6, 120.5, 106.8, 38.7, 32.1, 21.0, 13.2; MS ESI: calcd. For $C_{19}H_{21}BrN_3$ $[M+H]^+$, 372.09; found, 372.05.

4-Methyl-6-(2-(pyridin-3-yl)ethyl)pyridin-2-amine (11)—11 was synthesized according to general procedure **D** using **9** (48.0 mg) and $NH_2OH·HCl$ (46.9 mg). **11** was isolated as a brown oil (33.5 mg, 95%) after flash column chromatography (MeOH: DCM 3:7). ^1H NMR (500 MHz, Methanol-*d$_4$*): δ 8.93 (s, 1H), 8.80 (d, *J*= 6.0 Hz, 1H), 8.66 (d, *J*= 8.0 Hz, 1H), 8.09 (dd, *J* = 8.0, 6.0 Hz, 1H), 6.72 (s, 1H), 6.70 (s, 1H), 3.36–3.33 (m, 2H), 3.18–3.15 (m, 2H), 2.37 (s, 3H); ^{13}C NMR (125 MHz, methanol-*d$_4$*): δ 157.7, 154.6, 147.0, 146.9, 141.2, 140.7, 139.7, 127.2, 113.7, 110.0, 32.6, 31.0, 20.6; HRMS ESI: calcd. For $C_{13}H_{16}N_3$ $[M+H]^+$, 214.1339; found, 214.1337.

General Procedure B: Preparation of 13a-13e and 13g (Buchwald-Hartwig Palladium-Catalyzed Amination of 10)

A microwave vial was charged with Pd$_2$(dba)$_3$(5 mol%), Davephos (10 mol%), NaO^{t}Bu (1.2 equiv.), **10** (1 equiv.) and amine **12a-12f** (1.5–2 equiv.). The mixtures were diluted with dioxane to form a 0.16 M solution. The microwave vial was then capped, and the reaction mixture was stirred at 100 °C for 20 h. At this time, the cap was removed, and the reaction mixture was filtered through a silica pad. The filtrate was concentrated under reduced pressure and purified by flash column chromatography to give **13a-13e** and **13g**.

5-(2-(6-(2,5-Dimethyl-1*H*-pyrrol-1-yl)-4-methylpyridin-2-yl)ethyl)-*N*,*N*-dimethylpyridin-3-amine (13a)—Compound **13a** was synthesized according to general procedure **B** using Pd$_2$(dba)$_3$ (12.1 mg), Davephos (10.2 mg), NaO^{t}Bu (29.2 mg), **10** (93.3 mg), and amine **12a** (0.25 ml, 2M in THF). **13a** was isolated as a yellow oil (42.3 mg, 50%) after flash column chromatography (MeOH: DCM 1:19). ^{1}H NMR (500 MHz, CDCl$_3$): δ 7.95 (s, 1H), 7.79 (s, 1H), 6.90 (s, 1H), 6.84 (s, 1H), 6.77 (s, 1H), 5.86 (s, 2H), 3.07–3.03 (m, 2H), 3.02–2.98 (m, 2H), 2.91 (s, 6H), 2.34 (s, 3H), 2.10 (s, 6H); ^{13}C NMR (125 MHz, CDCl$_3$): δ 160.4, 151.7, 149.6, 146.1, 137.6, 136.7, 132.6, 128.5, 122.7, 120.2, 119.2, 106.8, 40.1, 39.4, 33.1, 21.0, 13.2.

2-(2,5-Dimethyl-1*H*-pyrrol-1-yl)-4-methyl-6-(2-(5-(piperidin-1-yl)pyridin-3-yl)ethyl)pyridine (13b)—Compound **13b** was synthesized according to general procedure **B** using Pd$_2$(dba)$_3$ (13.2 mg), Davephos (10.8 mg), NaO^{t}Bu (32.1 mg), **10** (102 mg, 0.28 mmol), and amine **12b** (46.8. mg, 0.55 mmol). **13b** was isolated as a yellow oil (73.2 mg, 71%) after flash column chromatography (ethyl acetate: hexanes 8:1). ^{1}H NMR (500 MHz, CDCl$_3$): δ 8.10 (s, 1H), 7.85 (s, 1H), 6.97 (s, 1H), 6.87 (s, 1H), 6.84 (s, 1H), 5.86 (s, 2H), 3.12 (t, J = 5.0 Hz, 4H), 3.06–2.98 (m, 4H), 2.34 (s, 3H), 2.10 (s, 6H), 1.68–1.64 (m, 4H), 1.59–1.54 (m, 2H); ^{13}C NMR (125 MHz, CDCl$_3$): δ 160.3, 151.8, 149.6, 147.6, 139.4, 136.9, 136.0, 128.4, 123.2, 122.8, 120.2, 106.8, 49.8, 39.3, 32.9, 25.5, 24.1, 21.0, 13.3.

4-(5-(2-(6-(2,5-Dimethyl-1*H*-pyrrol-1-yl)-4-methylpyridin-2-yl)ethyl)pyridin-3-yl)morpholine (13c)—Compound **13c** was synthesized according to general procedure **B** using Pd$_2$(dba)$_3$ (11.4 mg), Davephos (9.6 mg), NaO^{t}Bu (28.2 mg), **10** (88.1 mg), and amine **12c** (44.2 mg). **13c** was isolated as a yellow oil (86.6 mg, 96%) after flash column chromatography (MeOH: DCM 1:19). ^{1}H NMR (500 MHz, CDCl$_3$): δ 8.07 (s, 1H), 7.92 (s, 1H), 6.96 (s, 1H), 6.88 (s, 1H), 6.84 (s, 1H), 5.87 (s, 2H), 3.82 (t, J = 5.0 Hz, 4H), 3.11 (t, J = 5.0 Hz, 4H), 3.08–3.06 (m, 4H), 2.35 (s, 3H), 2.09 (s, 6H); ^{13}C NMR (125 MHz, CDCl$_3$): δ 160.2, 151.7, 149.6, 146.7, 141.2, 136.8, 136.0, 128.4, 122.7, 122.4, 120.2, 106.8, 66.7, 48.6, 39.2, 32.8, 21.0, 13.3; MS ESI: calcd. For C$_{23}$H$_{29}$N$_4$O [M+H]$^+$, 377.23; found, 377.18.

5-(2-(6-(2,5-Dimethyl-1*H*-pyrrol-1-yl)-4-methylpyridin-2-yl)ethyl)-*N*-(2-methoxyethyl)-*N*-methylpyridin-3-amine (13d)—Compound **13d** was synthesized according to general procedure **B** using Pd$_2$(dba)$_3$ (12.0 mg), Davephos (10.1 mg), NaO^{t}Bu (29.4 mg), **10** (93.5 mg, 0.25 mmol), and amine **12d** (46.1 mg). **13d** was isolated as a yellow oil (61.8 mg, 65%) after flash column chromatography (MeOH: DCM 1:19). ^{1}H NMR (500 MHz, CDCl$_3$): δ 7.95 (s, 1H), 7.70 (s, 1H), 6.90 (s, 1H), 6.84 (s, 1H), 6.77 (s, 1H), 5.86 (s, 2H), 3.52–3.50 (m, 2H), 3.47–3.45 (m, 2H), 3.32 (s, 3H), 3.07–3.03 (m, 2H), 3.00–2.97 (m, 2H), 2.93 (s, 3H), 2.34 (s, 3H), 2.10 (s, 6H); ^{13}C NMR (125 MHz, CDCl$_3$): δ 160.5, 151.7, 149.6, 145.0, 137.7, 136.7, 132.6, 128.4, 122.7, 120.2, 118.7, 106.8, 70.1, 59.1, 52.1, 39.4, 38.6, 33.1, 21.0, 13.2.

5-(2-(6-(2,5-Dimethyl-1*H*-pyrrol-1-yl)-4-methylpyridin-2-yl)ethyl)-*N*-(3-methoxypropyl)pyridin-3-amine (13e)—Compound **13e** was synthesized according to general procedure **B** using Pd$_2$(dba)$_3$ (12.0 mg), Davephos (10.2 mg), NaO^{t}Bu (29.5 mg), **10**

(94 mg), and amine **12e** (46.3 mg). **13e** was isolated as a yellow oil (66.5 mg, 70%) after flash column chromatography (MeOH: DCM 1:19). ^{1}H NMR (500 MHz, CDCl$_3$): δ 7.82 (s, 1H), 7.73 (s, 1H), 6.89 (s, 1H), 6.83 (s, 1H), 6.66 (s, 1H), 5.85 (s, 2H), 4.06 (brs, 1H), 3.47 (t, J = 6.0 Hz, 2H), 3.32 (s, 3H), 3.16 (t, J = 6.5 Hz, 2H), 3.04–3.01 (m, 2H), 2.96–2.93 (m, 2H), 2.33 (s, 3H), 2.09 (s, 6H), 1.86–1.81(m, 2H); ^{13}C NMR (125 MHz, CDCl$_3$): δ 160.5, 151.7, 149.6, 149.5, 138.5, 134.0, 133.9, 128.4, 122.7, 120.2, 118.5, 106.7, 71.2, 58.8, 41.6, 39.3, 32.9, 29.2, 21.0, 13.2; MS ESI: calcd. For C$_{23}$H$_{29}$N$_4$O [M+H]$^+$, 379.25; found, 379.20.

1-(5-(2-(6-(2,5-Dimethyl-1*H***-pyrrol-1-yl)-4-methylpyridin-2-yl)ethyl)pyridin-3-yl)-4-m ethylpiperazine (13g)**—Compound **13g** was synthesized by methylation of **13f**. Compound **13f** was prepared according to general procedure **B** using Pd$_2$(dba)$_3$ (28.1 mg), Davephos (24.1 mg), NaO^{t}Bu (70.7 mg), **10** (226.2 mg), and piperazine **12f** (105.4 mg). Crude product **13f** was subjected to methylation without purification. A scintillation vial was charged with **13f** (1 equiv.). The crude product was diluted with THF to form a 0.1 M solution followed by addition of triethylamine (1.5 equiv.) and MeI (1 equiv.). The reaction mixture was allowed to stir at r.t. for 1 h. The crude product was diluted with DCM and washed with water and brine. The organic layer was dried with Na$_2$SO$_4$ and concentrated under reduced pressure. The crude product mixture was purified by flash column chromatography (MeOH: DCM 1:6) to give **13g** (34.6 mg, 15% for the two steps). ^{1}H NMR (500 MHz, CDCl$_3$): δ 8.09 (s, 1H), 7.89 (s, 1H), 6.97 (s, 1H), 6.87 (s, 1H), 6.83 (s, 1H), 5.84 (s, 2H), 3.20 (t, J = 5.0 Hz, 4H), 3.04–2.99 (m, 4H), 2.60 (t, J = 5.0 Hz, 4H), 2.36 (s, 3H), 2.33 (s, 3H), 2.08 (s, 6H); ^{13}C NMR (125 MHz, CDCl$_3$): δ 160.2, 151.7, 149.6, 146.6, 140.9, 136.8, 136.3, 128.4, 122.8, 122.7, 120.3, 106.8, 54.7, 48.1, 45.9, 39.2, 32.9, 21.0, 13.2.

tert*-Butyl-4-(5-(2-(6-(2,5-dimethyl-1H***-pyrrol-1-yl)-4-methylpyridin-2-yl)ethyl)pyridi n-3-yl)-5,6-dihydropyridine-1(2***H***)-carboxylate (13h)**—A microwave vial was charged with Pd(OAc)$_2$ (13.4 mg), SPhos (41.1 mg), K$_3$PO$_4$ (849.1 mg), boronic acid **12f** (459.2 mg), and **10** (364 mg, 1.0 mmol). The mixture was diluted with toluene/water (20:1) to form a 0.13 M solution. The microwave vial was capped, and the reaction mixture was stirred at 100 °C for 20 h. The cap was removed, and the reaction mixture was diluted with ethyl acetate. The crude product was filtered, the filtrate was dried over Na$_2$SO$_4$, and concentrated under reduced pressure. **13h** was isolated as a yellow oil (316.2 mg, 68%) after flash column chromatography (ethyl acetate: hexanes 1:1). ^{1}H NMR (500 MHz, CDCl$_3$): δ 8.43 (s, 1H), 8.27 (s, 1H), 7.44 (s, 1H), 6.87 (s, 1H), 6.84 (s, 1H), 6.02–6.01 (m, 1H), 5.86 (s, 2H), 4.07–4.05 (m, 2H), 3.62–3.60 (m, 2H), 3.08–3.07 (m, 4H), 2.45–2.43 (m, 2H), 2.34 (s, 3H), 2.08 (s, 6H), 1.47 (s, 9H); ^{13}C NMR (125 MHz, CDCl$_3$): δ 159.9, 154.8, 151.8, 149.7, 148.3, 148.2, 144.1, 136.4, 135.8, 132.7, 132.6, 128.4, 122.7, 120.3, 106.8, 79.9, 39.1, 39.0, 32.6, 32.5, 28.5, 27.1, 21.0, 13.2.

General Procedure C: Preparation of 13i and 13k (Sonagashira-Cross Coupling of 10)

A microwave vial was charged with Pd(PPh$_3$)$_4$ (5 mol%), CuI (5 mol%), and **10** (1 equiv.). The mixtures were diluted with triethylamine to form a 0.16 M solution followed by the addition of alkyne (1.5–2 equiv.). The microwave vial was capped, and the reaction mixture

was stirred at 90 °C for 20 h. The cap was removed, and the reaction mixture was diluted with ethyl acetate and filtered. The filtrate was washed with water, ammonium chloride, and brine, dried with Na_2SO_4, and concentrated under reduced pressure. The crude product mixture was purified by flash column chromatography to give **13i** and **13k**.

tert-Butyl-3-(5-(2-(6-(2,5-dimethyl-1H-pyrrol-1-yl)-4-methylpyridin-2-yl)ethyl)pyridi n-3-yl)prop-2-ynyl(methyl)carbamate (13i)—Compound **13i** was synthesized according to general procedure **C** using $Pd(PPh_3)_4$ (28.8 mg), CuI (4.9 mg), alkyne **12i** (126.8 mg, 0.75 mmol), and **10** (184.6 mg, 0.50 mmol). **13i** was isolated as a brown oil (171.9 mg, 75%) after flash column chromatography (MeOH: DCM 1:19). ^{1}H NMR (500 MHz, $CDCl_3$): δ 8.44 (s, 1H), 8.29 (s, 1H), 7.50 (s, 1H), 6.86 (s, 1H), 6.84 (s, 1H), 5.86 (s, 2H), 4.26 (brs, 2H), 3.05–3.04 (m, 4H), 2.94 (s, 3H), 2.33 (s, 3H), 2.08 (s, 6H), 1.46 (s, 9H); ^{13}C NMR (125 MHz, $CDCl_3$): δ 159.7, 151.8, 150.1, 149.7, 149.0, 148.6, 148.1, 138.6, 128.4, 122.7, 120.4, 119.6, 106.8, 88.0, 80.3, 80.2, 38.9, 38.8, 33.6, 32.3, 28.4, 21.0, 13.2; MS ESI: calcd. For $C_{28}H_{35}N_4O_2$ $[M+H]^+$, 459.28; found, 459.20.

3-(5-(2-(6-(2,5-Dimethyl-1H-pyrrol-1-yl)-4-methylpyridin-2-yl)ethyl)pyridin-3-yl)-N, N-dimethylprop-2-yn-1-amine (13k)—Compound **13k** was synthesized according to general procedure **C** using $Pd(PPh_3)_4$ (28.8 mg), CuI (5.1 mg), alkyne **12k** (62.3. mg), and **10** (185 mg). **13k** was isolated as a brown oil (166.6 mg, 90%) after flash column chromatography (MeOH: DCM 1: 9). ^{1}H NMR (500 MHz, $CDCl_3$): δ 8.45 (s, 1H), 8.27 (s, 1H), 7.49 (s, 1H), 6.85 (s, 1H), 6.83 (s, 1H), 5.85 (s, 2H), 3.43 (s, 2H), 3.05–3.04 (m, 4H), 2.33 (s, 6H), 2.32 (s, 3H), 2.08 (s, 6H); ^{13}C NMR (125 MHz, $CDCl_3$): δ 159.8, 151.8, 150.1, 149.7, 148.8, 138.6, 136.2, 128.4, 122.7, 120.4, 119.9, 106.7, 88.0, 82.1, 48.6, 44.3, 38.9, 32.3, 21.0, 13.2; MS ESI: calcd. For $C_{24}H_{29}N_4$ $[M+H]^+$, 373.24; found, 373.19.

General Procedure D: Preparation of 11, 14a-14e, and 14g, (Pyrrole Deprotection)

A microwave vial was charged with **9**, **13a-13e**, or **13g** (1 equiv.) and $NH_2OH \cdot HCl$ (3–4 equiv.). The mixtures were diluted with EtOH/water (2:1) to form a 0.16 M solution. The microwave vial was capped, and the reaction mixture was stirred at 100 °C for 20 h. The cap was removed, and the reaction mixture was concentrated under reduced pressure. The crude product mixture was purified by flash chromatography to give **11, 14a-14e,** and **14g**.

6-(2-(5-(Dimethylamino)pyridin-3-yl)ethyl)-4-methylpyridin-2-amine (14a)—**14a** was synthesized according to general procedure **D** using **13a** (62.3 mg) and $NH_2OH \cdot HCl$ (52.7 mg). **14a** was isolated as a brown oil (47.2 mg, 99%) after flash column chromatography (MeOH: DCM 4:6). ^{1}H NMR (500 MHz, methanol-d_4): δ 8.02 (s, 1H), 7.96 (s, 1H), 7.70 (s, 1H), 6.68 (s, 1H), 6.66 (s, 1H), 3.19–3.15 (m, 2H), 3.12–3.08 (m, 8H), 2.36 (s, 3H); ^{13}C NMR (125 MHz, Methanol-d_4): δ 157.6, 154.6, 148.1, 147.5, 139.6, 127.6, 125.4, 123.6, 113.7, 109.8, 38.7, 32.2, 31.4, 20.5; HRMS ESI: calcd. For $C_{15}H_{21}N_4$ $[M+H]^+$, 257.1761; found, 251.1766.

4-Methyl-6-(2-(5-(piperidin-1-yl)pyridin-3-yl)ethyl)pyridin-2-amine (14b)—**14b** was synthesized according to general procedure **D** using **13b** (62.8 mg) and $NH_2OH \cdot HCl$ (28.0 mg). **14b** was isolated as a brown oil (32.3 mg, 65%) after flash column

chromatography (MeOH: DCM 1:9). ^{1}H NMR (500 MHz, methanol-d_4): δ 8.18 (s, 1H), 7.96 (s, 1H), 7.76 (s, 1H), 6.70 (s, 1H), 6.66 (s, 1H), 3.37 (t, J = 5.0 Hz, 4H), 3.16–3.12 (m, 2H), 3.10–3.06 (m, 2H), 2.35 (s, 3H), 1.71–1.68 (m, 6H); ^{13}C NMR (125 MHz, methanol-d_4): δ 157.5, 154.5, 148.5, 147.7, 138.7, 131.6, 128.8, 126.7, 113.7, 109.7, 48.2, 33.4, 31.4, 24.8, 23.6, 20.5; HRMS ESI: calcd. For $C_{18}H_{25}N_4$ [M+H]$^+$, 297.2074; found, 297.2078.

4-Methyl-6-(2-(5-morpholinopyridin-3-yl)ethyl)pyridin-2-amine (14c)—14c was synthesized according to general procedure **D** using **13c** (82.8 mg, 0.50 mmol) and NH$_2$OH·HCl (62.1 mg). **14c** was isolated as a brown oil (64.3 mg, 98%) after flash column chromatography (MeOH: DCM 3:7). ^{1}H NMR (500 MHz, methanol-d_4): δ 8.31 (s, 1H), 8.17 (s, 1H), 8.14 (s, 1H), 6.72 (s, 1H), 6.71 (s, 1H), 3.86 (t, J = 5.0 Hz, 4H), 3.43 (t, J = 5.0 Hz, 4H), 3.25–3.22 (m, 2H), 3.15–3.12 (m, 2H), 2.37 (s, 3H); ^{13}C NMR (125 MHz, methanol-d_4): δ 157.7, 154.5, 149.1, 147.2, 140.5, 129.3, 129.2, 125.2, 113.8, 109.9, 65.8, 46.6, 33.0, 31.4, 20.6; HRMS ESI: calcd. For $C_{17}H_{23}N_4O$ [M+H]$^+$, 299.1866; found, 299.1872.

6-(2-(5-((2-Methoxyethyl)(methyl)amino)pyridin-3-yl)ethyl)-4-methylpyridin-2-amine (14d)—14d was synthesized according to general procedure **D** using **13d** (61.8 mg) and NH$_2$OH·HCl (45.9 mg). **14d** was isolated as a brown oil (48.3 mg, 98%) after flash column chromatography (MeOH: DCM 3:7). ^{1}H NMR (500 MHz, methanol-d_4): δ 8.11 (s, 1H), 8.01 (s, 1H), 7.87 (s, 1H), 6.73 (s, 1H), 6.71 (s, 1H), 3.72 (t, J = 5.0 Hz, 2H), 3.63 (t, J = 5.0 Hz, 2H), 3.32 (s, 3H), 3.23–3.20 (m, 2H), 3.15–3.12 (m, 5H), 2.36 (s, 3H); ^{13}C NMR (125 MHz, methanol-d_4): δ 157.7, 154.5, 147.9, 147.3, 140.0, 126.6, 126.5, 122.9, 113.8, 109.9, 70.0, 58.0, 51.4, 37.6, 33.1, 31.3, 20.6; HRMS ESI: calcd. For $C_{17}H_{25}N_4O$ [M+H]$^+$, 301.2023; found, 301.2031.

6-(2-(5-(3-Methoxypropylamino)pyridin-3-yl)ethyl)-4-methylpyridin-2-amine (14e)—14e was synthesized according to general procedure **D** using **13e** (66.5 mg) and NH$_2$OH·HCl (50.2 mg.). **14e** was isolated as a brown oil (49.1 mg, 93%) after flash column chromatography (MeOH: DCM 3:7). ^{1}H NMR (500 MHz, methanol-d_4): δ 7.95 (s, 1H), 7.93 (s, 1H), 7.65 (s, 1H), 6.71 (s, 1H), 6.68 (s, 1H), 3.51 (t, J = 6.0 Hz, 2H), 3.35 (s, 3H), 3.29 (t, J = 7.0 Hz, 2H), 3.18–3.15 (m, 2H), 3.12–3.09 (m, 2H), 2.36 (s, 3H), 1.92–1.87 (m, 2H); ^{13}C NMR (125 MHz, methanol-d_4): δ 157.7, 154.5, 148.0, 147.2, 140.4, 127.0, 126.4, 122.4, 113.8, 109.9, 69.6, 57.6, 39.6, 32.9, 31.2, 28.3, 20.6; HRMS ESI: calcd. For $C_{17}H_{25}N_4O$ [M+H]$^+$, 301.2023; found, 301.2026.

4-Methyl-6-(2-(5-(4-methylpiperazin-1-yl)pyridin-3-yl)ethyl)pyridin-2-amine (14g)—14g was synthesized according to general procedure **D** using **13g** (34.6 mg) and NH$_2$OH·HCl (25.1 mg). **14g** was isolated as a brown oil (18.0 mg, 65%) after flash column chromatography (MeOH: DCM 4:6). ^{1}H NMR (500 MHz, methanol-d_4): δ 8.16 (s, 1H), 7.92 (s, 1H), 7.42 (s, 1H), 6.59 (s, 1H), 6.55 (s, 1H), 3.51–3.49 (m, 4H), 3.28–3.26 (m, 4H), 3.05–2.98 (m, 4H), 2.84 (s, 3H), 2.31 (s, 3H); ^{13}C NMR (125 MHz, methanol-d_4): δ 156.2, 155.3, 149.8, 146.3, 140.1, 136.6, 135.7, 123.9, 113.6, 109.1, 53.3, 46.1, 42.8, 34.5, 31.6, 20.4; HRMS ESI: calcd. For $C_{18}H_{26}N_5$ [M+H]$^+$, 312.2183; found, 312.2186.

General Procedure E: Preparation of 14j and 14k (Alkyne Reduction and Pyrrole Deprotection)

A scintillation vial was charged with 10% wt. Pd/C and **13k** (1 equiv.). The mixtures were diluted with methanol to form a 0.1 M solution. The reaction mixture was stirred at r.t. for 20 h under hydrogen gas. At this time, the crude was filtered, and the filtrate was concentrated under reduced pressure. The crude product was subjected to 2,5-dimethylpyrrole deprotection as described above (general procedure **D**) without purification. A microwave vial was charged with the hydrogenation crude product (1 equiv.) and $NH_2OH \cdot HCl$ (3–4 equiv.). The mixtures were diluted with EtOH/water (2:1) to form a 0.16 M solution. The microwave vial was capped, and the reaction mixture was stirred at 100 °C for 20 h. The cap was removed, and the reaction mixture was concentrated under reduced pressure. The crude product mixture was purified by flash chromatography to give **14k**.

6-(2-(5-(3-(Dimethylamino)propyl)pyridin-3-yl)ethyl)-4-methylpyridin-2-amine (14k)—**14k** was synthesized according to general procedure **E** using **13k** (166.6 mg), 10% wt. Pd/C (131.2 mg), and $NH_2OH \cdot HCl$ (79.2 mg). **14k** was isolated as a brown oil (118.5 mg, 89%) after flash column chromatography (MeOH: DCM 4:6). ^1H NMR (500 MHz, methanol-d_4): δ 8.80 (s, 2H), 8.71 (s, 1H), 6.76 (s, 2H), 3.36–3.33 (m, 2H), 3.31–3.28 (m, 2H), 3.22–3.19 (m, 2H), 3.03–3.00 (m, 2H), 2.95 (s, 6H), 2.38 (s, 3H), 2.27–2.21 (m, 2H); ^{13}C NMR (125 MHz, methanol-d_4): δ 157.8, 154.5, 147.1, 147.0, 141.1, 140.4, 139.4, 139.1, 113.9, 110.0, 56.5, 42.2, 32.7, 31.1, 28.7, 24.8, 20.7; HRMS ESI: calcd. For $C_{18}H_{27}N_4$ [M+H]$^+$, 299.2230; found, 299.2236.

4-Methyl-6-(2-(5-(3-(methylamino)propyl)pyridin-3-yl)ethyl)pyridin-2-amine (14j)—**14j** was synthesized by Boc deprotection of **13i** followed by general procedure **E**. Compound **13i** (171.9 mg, 0.38 mmol) was diluted with DCM (3.8 ml) to form a 0.1 M solution followed by addition of TFA (0.8 mL). The reaction mixture was allowed to stir at r.t. for 1 h. The crude product was concentrated under reduced pressure, diluted with DCM, and washed with sat. $NaHCO_3$. The organic layer was dried over Na_2SO_4 and concentrated to give crude product **13j**. The crude product was used for further steps without purification. **14j** was synthesized according to general procedure **E** using **13j** (82.6 mg), 10% wt. Pd/C (56.1 mg), and $NH_2OH \cdot HCl$ (52.2 mg). **14j** was isolated as a brown oil (63.8 mg, 60%) after flash column chromatography (MeOH: DCM 4:6). ^1H NMR (500 MHz, methanol-d_4): δ 8.79 (s, 1H), 8.78 (s, 1H), 8.68 (s, 1H), 6.75 (s, 2H), 3.35–3.32 (m, 2H), 3.21–3.18 (m, 2H), 3.14–3.11 (m, 2H), 3.04–3.01 (m, 2H), 2.75 (s, 6H), 2.38 (s, 3H), 2.20–2.14 (m, 2H); ^{13}C NMR (125 MHz, methanol-d_4): δ 157.8, 154.5, 147.1, 147.0, 141.2, 140.4, 139.4, 139.2, 113.9, 110.0, 48.1, 32.7, 32.4, 31.1, 28.8, 26.3, 20.7; HRMS ESI: calcd. For $C_{17}H_{25}N_4$ [M+H]$^+$, 285.2074; found, 285.2078.

4-Methyl-6-(2-(5-(1-methylpiperidin-4-yl)pyridin-3-yl)ethyl)pyridin-2-amine (14h)—**14h** was synthesized by alkyne reduction of **13h** followed by Boc reduction and pyrrole deprotection. **13h** (316.2 mg) was treated with 10% wt. Pd/C (235.2 mg) and diluted with MeOH to form a 0.1 M solution. The reaction mixture was stirred at r.t. for 20 h under hydrogen gas. The crude product was filtered through Celite, and the filtrate was concentrated under reduced pressure. The crude product (298.9 mg) was subjected to *tert-*

butyl carbamate reduction without purification. A round-bottom flask was charged with lithium aluminum hydride (126.1 mg), and the hydrogenation crude product solution in THF (0.1 M) was slowly added at 0 °C under N_2. The reaction mixture was allowed to warm up to r.t., refluxed for 1 h, quenched, with water, filtered, and extracted with dichloromethane to give the crude *tert*-butyl carbamate reduction product (136.6 mg)., which was treated with $NH_2OH \cdot HCl$ (99.7 mg) and diluted with EtOH/water (2:1) to form a 0.16 M solution. The reaction mixture was stirred at 100 °C for 20 h, concentrated under reduced pressure, and purified by flash column chromatography to give **14h** (74.4 mg, 36%) as a brown oil. ^1H NMR (500 MHz, methanol-d_4): δ 8.35 (s, 1H), 8.32 (s, 1H), 7.74 (s, 1H), 6.60 (s, 1H), 6.54 (s, 1H), 3.62–3.60 (m, 2H), 3.22–3.20 (m, 3H), 3.08–3.07 (m, 2H), 3.04–2.98 (m, 4H), 2.93 (s, 3H), 2.88–2.86 (m, 2H), 2.29 (s, 3H); ^{13}C NMR (125 MHz, methanol-d_4): δ 155.8, 155.6, 150.1, 147.4, 145.8, 139.7, 136.5, 135.4, 113.7, 109.0,54.1, 48.5, 42.5, 34.7, 31.6, 29.9, 20.4; HRMS ESI: calcd. For $C_{19}H_{27}N_4$ $[M+H]^+$, 311.2230; found, 311.2231.

NOS Enzyme Inhibition Assays

Enzyme inhibition was evaluated by measuring NO production with the hemoglobin capture assay, which was performed with purified NOSs in 96-well plates using a Biotek Gen5™ microplate reader. Purified NOSs used in this study, rat nNOS, human nNOS, murine macrophage iNOS, bovine eNOS, and human eNOS, are recombinant enzymes, expressed in *E.* coli and purified by reported procedures.[37–39] For rat and human nNOS, bovine and human eNOS, the assays were performed at 37 °C in 100 mM HEPES buffer with 10% glycerol (pH 7.4) in the presence of 10 μM *L*-arginine and tetrahydrobiopterin, 100 μM NADPH, 0.83 mM $CaCl_2$, 320 units/mL of calmodulin, and 3 μM human oxyhemoglobin. For iNOS, the assay was performed at 37 °C in HEPES buffer in the presence of *L*-arginine and cofactors (NADPH, H_4B, and human oxyhemoglobin). For all the assays, NO production was read by monitoring the absorbance at 401 nm, and kinetic readouts were recorded for 6 min. The inhibition constants (K_i) for all NOSs were calculated from the IC_{50} values and K_m (human nNOS: 1.6 μM; rat nNOS: 1.3 μM; murine iNOS: 8.2 μM; bovine eNOS: 1.7 μM; human eNOS: 3.9 μM)[40] using the Cheng–Prusoff equation: $K_i = IC_{50}/(1+ [S]/K_m)$.[41] IC_{50} values were determined with seven to nine concentration points (200 μM–50 nM) to construct dose–response curves, and were calculated by nonlinear regression using GraphPad Prism. The calculated standard deviations of the assays were less than 10% with all NOSs using dose-response curves.

Inhibitor Complex Crystal Preparation

The preparations of rat nNOS, bovine eNOS, human eNOS, and human nNOS heme domains used for crystallographic studies were carried out using procedures described previously.[24,42,43] The rat nNOS heme domain (at 9 mg/mL containing 20 mM histidine) or the bovine eNOS heme domain (at 10 mg/mL containing 2 mM imidazole) were used for the sitting drop vapor diffusion crystallization setup under conditions previously reported.[42] Human nNOS crystals were obtained with a triple K301R/R354A/G357D mutant heme domain at 10 mg/mL. By slightly modifying the original conditions where the monoclinic C2 crystals grew, a new crystal form belonging to the $P2_12_12_1$ space group was obtained. Long plate crystals were grown at 4 °C with the sitting drop setup against a well solution of 8–9% PEG3350, 40 mM citric acid, 60 mM Bis-Tris-Propane, pH 6.2, 10% glycerol, and 5

mM TCEP. New crystals belong to the orthorhombic $P2_12_12_1$ space group with cell dimensions of a= 52.3 Å, b= 122.7 Å, and c= 165.0 Å with one homodimer in the asymmetric unit, which closely resembles the cell dimensions of rat nNOS crystal. Fresh crystals were first passed stepwise through cryoprotectant solutions and then soaked with 10 mM inhibitor for 4–6 h at 4 °C before being flash cooled in liquid nitrogen.

X-ray Diffraction Data Collection, Data Processing, and Structural Refinement

The cryogenic (100 K) X-ray diffraction data were collected remotely at the Stanford Synchrotron Radiation Light source (SSRL) or Advanced Light Source (ALS) through the data collection control software Blu-Ice[44] and a crystal mounting robot. When a Q315r CCD detector was used, 90–100° of data were typically collected with 0.5° per frame. If a Pilatus pixel array detector was used, 120–130° of fine-sliced data were collected with 0.2° per frame. Raw CCD data frames were indexed, integrated, and scaled using MOSFLM,[45] but the pixel array data were processed with XDS[46] and scaled with or Aimless.[47] The binding of inhibitors was detected by the initial difference Fourier maps calculated with REFMAC.[48] The inhibitor molecules were then modeled in COOT[49] and refined using REFMAC or PHENIX.[50] Disordering in portions of inhibitors bound in the NOS active sites was often observed, sometimes resulting in poor density quality. However, partial structural features usually could still be visible if the contour level of the sigma A weighted $2m|F_o|-D|F_c|$ map dropped to 0.5 σ, which afforded the building of reasonable models into the disordered regions. Water molecules were added in PHENIX and checked by COOT. The TLS[51] protocol was implemented in the final stage of refinements with each subunit as one TLS group. The omit F_o–F_c density maps shown in figures were calculated by running one round of simulated annealing refinement (initial temperature 2000 K) in PHENIX with the inhibitor coordinate removed from the input PDB file to generate map coefficients DELFWT and PHDELWT. The refined structures were validated in COOT before deposition in the RCSB protein data bank. The crystallographic data collection and structure refinement statistics are summarized in Table S1 of the Supporting Information, with the PDB accession codes included.

Supplementary Material

Refer to Web version on PubMed Central for supplementary material.

Acknowledgments

ABBREVIATIONS USED

NO   nitric oxide

nNOS	neuronal nitric oxide synthase
iNOS	inducible nitric oxide synthase
eNOS	endothelial nitric oxide synthase
HnNOS	human neuronal nitric oxide synthase
HeNOS	human endothelial nitric oxide synthase
L-Arg	L-arginine
FAD	flavin adenine dinucleotide
FMN	flavin mononucleotide
NADPH	reduced nicotinamide adenine dinucleotide phosphate
H₄B	$(6R)$-5,6,7,8-tetrahydrobiopterin
HEPES	4-(2-hydroxyethyl)-1-piperazine-ethanesulfonic acid
TCEP	tris(2-chloroethyl)phosphate
WT	wild type

References

1. Kerwin JF Jr, Lancaster JR Jr, Feldman PL. Nitric oxide: a new paradigm for second messengers. J Med Chem. 1995; 38:4343–4362. [PubMed: 7473563]

2. Palmer RM, Ferrige AG, Moncada S. Nitric oxide release accounts for the biological activity of endothelium-derived relaxing factor. Nature. 1987; 327:524–526. [PubMed: 3495737]

3. Ignarro LJ, Lippton H, Edwards JC, Baricos WH, Hyman AL, Kadowitz PJ, Gruetter CA. Mechanism of vascular smooth muscle relaxation by organic nitrates, nitrites, nitroprusside and nitric oxide: evidence for the involvement of S-nitrosothiols as active intermediates. J Pharmacol Exp Ther. 1981; 218:739–749. [PubMed: 6115052]

4. Vincent SR. Nitric oxide: a radical neurotransmitter in the central nervous system. Prog Neurobiol. 1994; 42:129–160. [PubMed: 7480785]

5. Bogdan C. Nitric oxide and the immune response. Nat Immunol. 2001; 2:907–916. [PubMed: 11577346]

6. Karpuzoglu E, Ahmed SA. Estrogen regulation of nitric oxide and inducible nitric oxide synthase (iNOS) in immune cells: implications for immunity, autoimmune diseases, and apoptosis. Nitric Oxide. 2006; 15:177–186. [PubMed: 16647869]

7. Roe ND, Ren J. Nitric oxide synthase uncoupling: a therapeutic target in cardiovascular diseases. Vascul Pharmacol. 2012; 57:168–172. [PubMed: 22361333]

8. Baranano DE, Snyder SH. Neural roles for heme oxygenase: contrasts to nitric oxide synthase. Proc Natl Acad Sci USA. 2001; 98:10996–11002. [PubMed: 11572959]

9. Steinert JR, Chernova T, Forsythe ID. Nitric oxide signaling in brain function, dysfunction, and dementia. Neuroscientist. 2010; 16:435–452. [PubMed: 20817920]

10. Huang H, Ji H, Li H, Jing Q, Labby KJ, Martasek P, Roman LJ, Poulos TL, Silverman RB. Selective monocationic inhibitors of neuronal nitric oxide synthase. Binding mode insights from molecular dynamics simulations. J Am Chem Soc. 2012; 134:11559–11572. [PubMed: 22731813]

11. Law A, Gauthier S, Quirion R. Say NO to Alzheimer's disease: the putative links between nitric oxide and dementia of the Alzheimer's type. Brain Res Brain Res Rev. 2001; 35:73–96. [PubMed: 11245887]

12. Aquilano K, Baldelli S, Rotilio G, Ciriolo MR. Role of nitric oxide synthases in Parkinson's disease: a review on the antioxidant and anti-inflammatory activity of polyphenols. Neurochem Res. 2008; 33:2416–26. [PubMed: 18415676]

13. Deckel AW, Tang V, Nuttal D, Gary K, Elder R. Altered neuronal nitric oxide synthase expression contributes to disease progression in Huntington's disease transgenic mice. Brain Res. 2002; 939:76–86. [PubMed: 12020853]

14. Yamanaka K, Chun SJ, Boillee S, Fujimori-Tonou N, Yamashita H, Gutmann DH, Takahashi R, Misawa H, Cleveland DW. Astrocytes as determinants of disease progression in inherited amyotrophic lateral sclerosis. Nat Neurosci. 2008; 11:251–253. [PubMed: 18246065]

15. Baek KJ, Thiel BA, Lucas S, Stuehr DJ. Macrophage nitric oxide synthase subunits. purification, characterization, and role of prosthetic groups and substrate in regulating their association into a dimeric enzyme. J Biol Chem. 1993; 268:21120–21129. [PubMed: 7691806]

16. Mukherjee P, Cinelli MA, Kang S, Silverman RB. Development of nitric oxide synthase inhibitors for neurodegeneration and neuropathic pain. Chem Soc Rev. 2014; 43:6814–6838. [PubMed: 24549364]

17. Alderton WK, Cooper CE, Knowles RG. Nitric oxide synthases: structure, function and inhibition. Biochem J. 2001; 357:593–615. [PubMed: 11463332]

18. Feng C. Mechanism of Nitric Oxide Synthase regulation: electron transfer and interdomain interactions. Coord Chem Rev. 2012; 256:393–411. [PubMed: 22523434]

19. Poulos TL, Li H. Structural basis for isoform-selective inhibition in nitric oxide synthase. Acc Chem Res. 2013; 46:390–398. [PubMed: 23030042]

20. Annedi SC, Ramnauth J, Maddaford SP, Renton P, Rakhit S, Mladenova G, Dove P, Silverman S, Andrews JS, Felice MD, Porreca F. Discovery of *cis-N*-(1-(4-(methylamino)cyclohexyl)indolin-6-yl)thiophene-2-carboximidamide: A 1,6-disubstituted indoline derivative as a highly selective inhibitor of human neuronal nitric oxide synthase (nNOS) without any cardiovascular liabilities. J Med Chem. 2012; 55:943–955. [PubMed: 22175766]

21. Suaifan GA, Shehadehh M, Al-Ijel H, Taha MO. Extensive ligand-based modeling and in silico screening reveal nanomolar inducible nitric oxide synthase (iNOS) inhibitors. J Mol Graph. 2012; 37:1–26.

22. Ji H, Tan S, Igarashi J, Li H, Derrick M, Martasek P, Roman LJ, Vasquez-Vivar J, Poulos TL, Silverman RB. Selective neuronal nitric oxide synthase inhibitors and the prevention of cerebral palsy. Ann Neurol. 2009; 65:209–217. [PubMed: 19235180]

23. Xue F, Fang J, Delker SL, Li H, Martasek P, Roman LJ, Poulos TL, Silverman RB. Symmetric double-headed aminopyridines, a novel strategy for potent and membrane-permeable inhibitors of neuronal nitric oxide synthase. J Med Chem. 2011; 54:2039–2048. [PubMed: 21410186]

24. Kang S, Li H, Tang W, Martasek P, Roman LJ, Poulos TL, Silverman RB. 2-Aminopyridines with a truncated side chain to improve human neuronal Nitric Oxide Synthase inhibitory potency and selectivity. J Med Chem. 2015; 58:5548–5560. [PubMed: 26120733]

25. Examples for amidine inhibitors: Zhang HQ, Fast W, Marletta MA, Martásek P, Silverman RB. Potent and selective inhibition of neuronal nitric oxide synthase by N^{ω}-propyl-L-arginine. J Med Chem. 1997; 40:3869–3870. [PubMed: 9397167]

26. Examples for dipeptide inhibitors: Ji H, Gómez-Vidal JA, Martásek P, Roman LJ, Silverman RB. Conformationally-restricted dipeptide amides as potent and selective neuronal nitric oxide synthase inhibitors. J Med Chem. 2006; 49:6254–6263. [PubMed: 17034131]

27. Examples for thiophene inhibitors: Huang H, Li H, Yang S, Chreifi G, Martásek P, Roman LJ, Meyskens FL, Poulos TL, Silverman RB. Potent and selective double-headed thiophene-2-carboximidamide inhibitors of neuronal nitric oxide synthase for the treatment of melanoma. J Med Chem. 2014; 57:686–700. [PubMed: 24447275]

28. Examples for aminopyridine inhibitors: Huang H, Li H, Martásek P, Roman LJ, Poulos TL, Silverman RB. Structure-guided design of selective inhibitors of neuronal nitric oxide synthase. J Med Chem. 2013; 56:3024–3032. [PubMed: 23451760]

29. Examples for aminoquinoline inhibitors: Cinelli MA, Li H, Chreifi G, Martásek P, Roman LJ, Poulos TL, Silverman RB. A simplified 2-aminoquinoline-based scaffold for potent and selective neuronal nitric oxide synthase inhibition. J Med Chem. 2014; 57:1513–1530. [PubMed: 24472039]

Cinelli MA, Li H, Pensa AV, Kang S, Roman LJ, Martasek P, Poulos TL, Silverman RB. Phenyl ether- and aniline-containing 2-aminoquinolines as potent and selective inhibitors of neuronal nitric oxide synthase. J Med Chem. 2015; 58:8694–8712. [PubMed: 26469213]

30. Examples for 2,4-disubstituted pyrimidines inhibitors: Mukherjee P, Li H, Sevrioukova I, Chreifi G, Martásek P, Roman LJ, Poulos TL, Silverman RB. Novel 2,4-disubstituted pyrimidines as potent, selective, and cell-permeable inhibitors of neuronal Nitric Oxide Synthase. J Med Chem. 2015; 58:1067–1088. [PubMed: 25489882]

31. Surry DS, Buchwald SL. Dialkylbiaryl phosphines in Pd-catalyzed amination: A user's guide. Chem Sci. 2011; 2:27–50. [PubMed: 22432049]

32. (a) Zhang M, Cui X, Chen X, Wang L, Li J, Wu Y, Hou L, Wu Y. Facile synthesis of aryl(het)cyclopropane catalyzed by palladacycle. Tetrahedron. 2012; 68:900–905.(b) Wallace DJ, Chen CY. Cyclopropyl boronic acid: synthesis and Suzuki cross-coupling reactions. Tetrahedron Lett. 2002; 43:6987–6990.

33. Nakamura H, Onagi S, Kamakura T. Synthesis of heterocyclic allenes *via* palladium-catalyzed hydride-transfer reaction of propargylic amines. J Org Chem. 2005; 70:2357–2360. [PubMed: 15760231]

34. Labby KJ, Xue F, Kraus JM, Ji H, Mataka J, Li H, Martásek P, Roman LJ, Poulos TL, Silverman RB. Intramolecular hydrogen bonding: A potential strategy for more bioavailable inhibitors of neuronal nitric oxide synthase. Bioorg Med Chem. 2012; 20:2435–2443. [PubMed: 22370337]

35. Hevel JM, Marletta MA. Nitric-oxide synthase assays. Methods Enzymol. 1994; 233:250–258. [PubMed: 7516999]

36. Li H, Jamal J, Plaza C, Pineda SH, Chreifi G, Jing Q, Cinelli MA, Silverman RB, Poulos TL. Crystal structures of human constitutive nitric oxide synthases. Acta Crystallogr Sect D: Biol Crystallogr. 2014; 70:2667–2674. [PubMed: 25286850]

37. Roman LJ, Sheta EA, Martásek P, Gross SS, Liu Q, Masters BSS. High-level expression of functional rat neuronal nitric oxide synthase in Escherichia coli. Proc Natl Acad Sci U S A. 1995; 92:8428–8432. [PubMed: 7545302]

38. Hevel JM, White KA, Marletta MA. Purification of the inducible murine macrophage nitric oxide synthase: identification as a flavor protein. J Biol Chem. 1991; 266:22789–22791. [PubMed: 1720773]

39. Gerber NC, Ortiz de Montellano PR. Neuronal nitric oxide synthase: expression in *Escherichia coli*, irreversible inhibition by phenyldiazene, and active site topology. J Biol Chem. 1995; 270:17791–17796. [PubMed: 7543092]

40. Delker SL, Xue F, Li H, Jamal J, Silverman RB, Poulos TL. Role of zinc in isoform-selective inhibitor binding to neuronal nitric oxide synthase. Biochemistry. 2010; 49:10803–10810. [PubMed: 21138269]

41. Cheng YC, Prusoff WH. Relationship between the inhibition constant (K_i) and the concentration of the inhibitor which causes 50% inhibition (IC_{50}) of an enzymatic reaction. Biochem Pharmacol. 1973; 22:3099–3108. [PubMed: 4202581]

42. Li H, Jamal J, Delker S, Plaza C, Ji H, Jing Q, Huang H, Kang S, Silverman RB, Poulos TL. The mobility of a conserved tyrosine residue controls isoform-dependent enzyme-inhibitor interaction in nitric oxide synthases. Biochemistry. 2014; 53:5272–5279. [PubMed: 25089924]

43. Labby KJ, Xue F, Kraus JM, Ji H, Mataka J, Li H, Martásek P, Roman LJ, Poulos TL, Silverman RB. Intramolecular hydrogen bonding: A potential strategy for more bioavailable inhibitors of neuronal nitric oxide synthase. Bioorg Med Chem. 2012; 20:2435–2443. [PubMed: 22370337]

44. McPhillips TM, McPhillips SE, Chiu HJ, Cohen AE, Deacon AM, Ellis PJ, Garman E, Gonzalez A, Sauter NK, Phizackerley RP, Soltis SM, Kuhn P. Blu-Ice and the distributed control system: software for data acquisition and instrument control at macromolecular crystallography beamlines. J Synchrotron Radiat. 2002; 9:401–406. [PubMed: 12409628]

45. Leslie, AGW.; Powell, HR. Processing diffraction data with Mosflm. In: Read, RJ.; Sussman, JL., editors. Evolving Methods for Macromolecular Crystallography. Vol. 245. Springer; the Netherlands: 2007. p. 41-51.

46. Kabsch W, XDS. Acta Crystallogr Sect D: Biol Crystallogr. 2010; D66:125–132. [PubMed: 20124692]

47. Evans PR. Scaling and assessment of data quality. Acta Crystallogr Sect D: Biol Crystallogr. 2006; D62:72–82. [PubMed: 16369096]

48. Murshudov GN, Vagin AA, Dodson EJ. Refinement of macromolecular structures by the maximum-likelihood method. Acta Crystallogr Sect D: Biol Crystallogr. 1997; D53:240–255. [PubMed: 15299926]

49. Emsley P, Cowtan K. Coot: model-building tools for molecular graphics. Acta Crystallogr Sect D: Biol Crystallogr. 2004; D60:2126–2132. [PubMed: 15572765]

50. Adams PD, Afonine PV, Bunkóczi G, Chen VB, Davis IW, Echols N, Headd JJ, Hung L-W, Kapral GJ, Grosse-Kunstleve RW, McCoy AJ, Moriarty NW, Oeffner R, Read RJ, Richardson DC, Richardson JS, Terwilliger TC, Zwart PH. PHENIX: a comprehensive Python-based system for macromolecular structure solution. Acta Crystallogr. 2010; D66:213–221.

51. Winn MD, Isupov MN, Murshudov GN. Use of TLS parameters to model anisotropic displacements in macromolecular refinement. Acta Crystallogr Sect D: Biol Crystallogr. 2001; D57:122–133. [PubMed: 11134934]
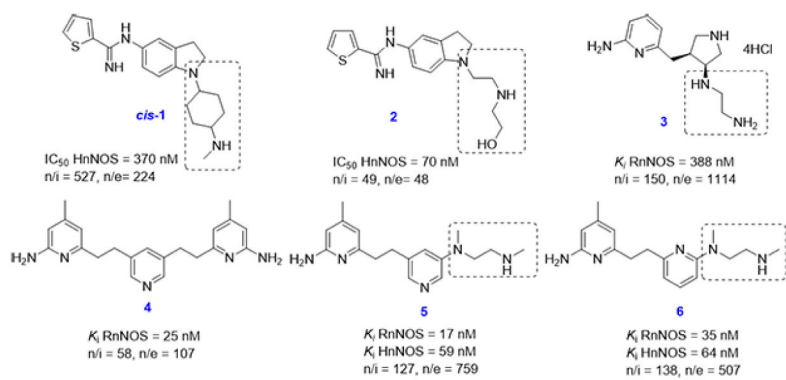
Figure 1.
Representative nNOS inhibitors that share similar pharmacophores
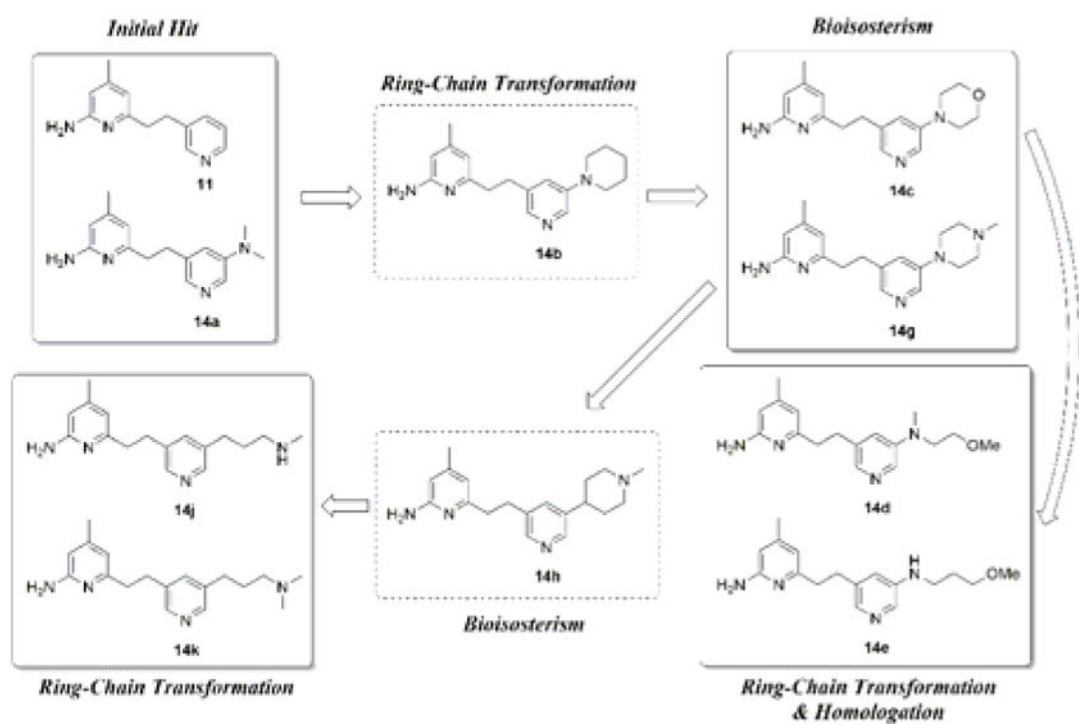
Figure 2.
nNOS inhibitors design strategy in this study
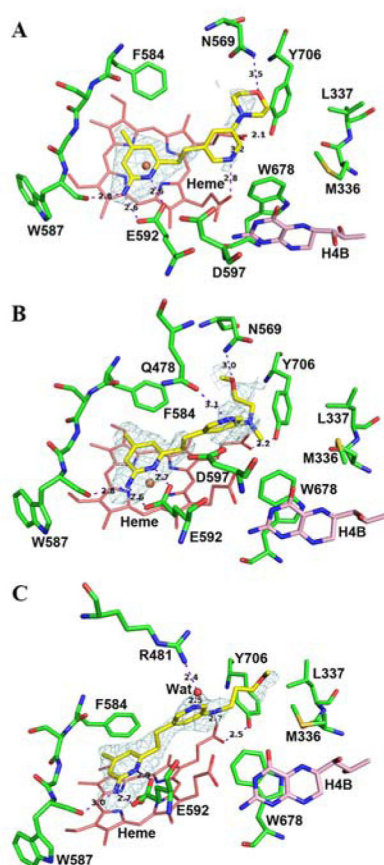
Figure 3.
Active site structure of **14c** (**A**) (PDB 5FVP), **14d** (**B**) (PDB 5FW0) or **14e** (**C**) (PDB 5FVO)
bound to nNOS. The omit $F_o - F_c$ electron density for the inhibitor is shown at the 2.5 σ
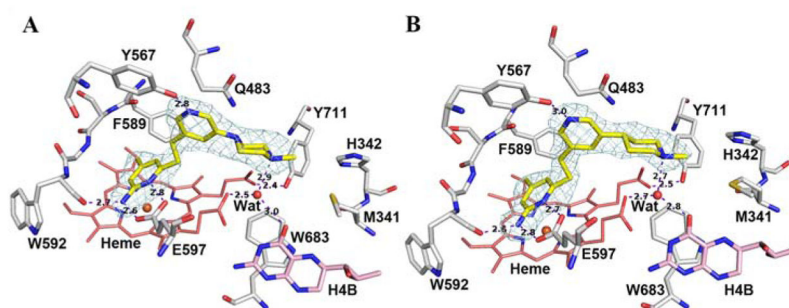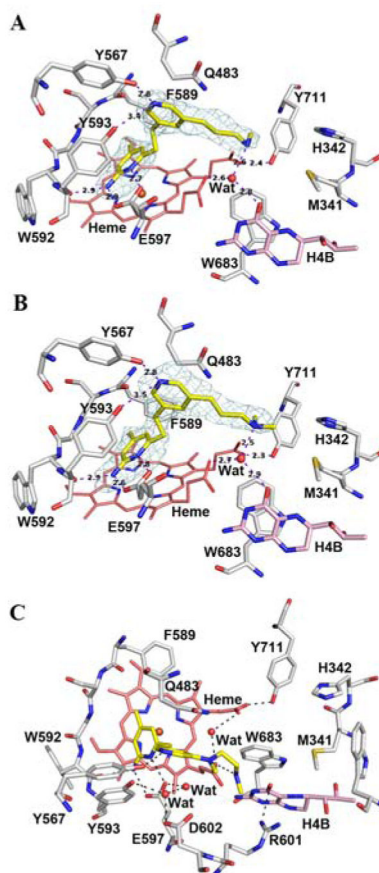contour level. Major hydrogen bonds are depicted with dashed lines and distances are shown
in Å.
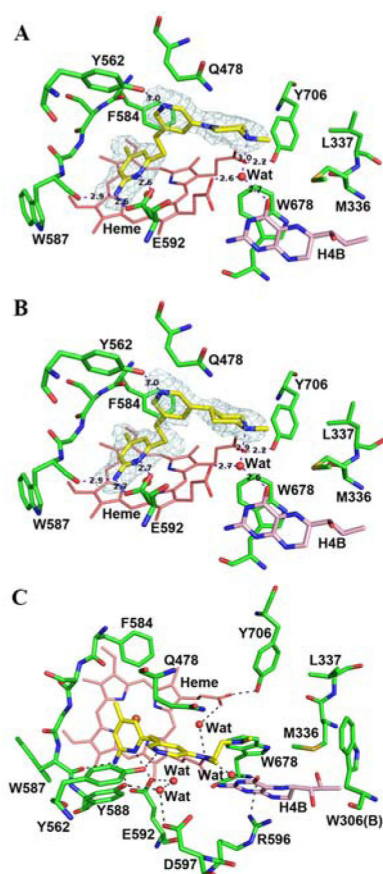
Figure 4.

Active site structure of **14g** (**A**) (PDB 5FVQ) or **14h** (**B**) (PDB 5FVR) bound to nNOS. The omit $F_o - F_c$ electron density for the inhibitor is shown at the 2.5 σ contour level. Major hydrogen bonds are depicted with dashed lines and distances are marked in Å. For comparison, panel **C** also shows the active site structure of **5** (PDB 4UH1) bound to nNOS.
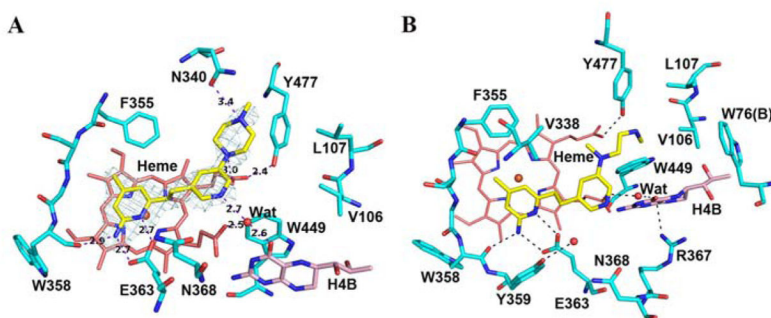
Figure 5.
(**A**) Active site structure of **14g** (PDB 5FVY) bound to bovine eNOS. The omit $F_o - F_c$ electron density for the inhibitor is shown at the 2.5 σ contour level. (**B**) Active site structure of **5** (PDB 4UH8) bound to bovine eNOS. Major hydrogen bonds are depicted with dashed lines, and distances are marked in Å.
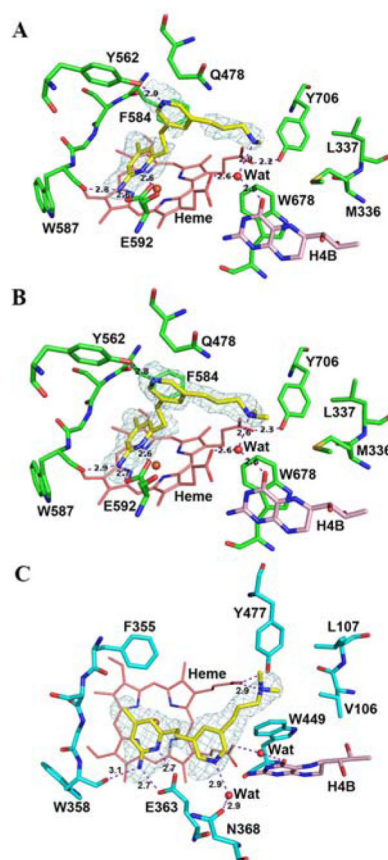
Figure 6.
Active site structure of **14j** (**A**) (PDB 5FVS) or **14k** (**B**) (PDB 5FVT) bound to nNOS.
Active site structure of **14k** (**C**) (PDB 5FVZ) bound to eNOS. The omit $F_o - F_c$ electron density for the inhibitor is shown at the 2.5 σ contour level. Major hydrogen bonds are depicted with dashed lines, and distances are marked in Å.

Figure 7.
Active site structure of **14g** (**A**) (PDB 5FVU) or **14h** (**B**) (PDB 5FVV) bound to human nNOS. The omit $F_o - F_c$ electron density for the inhibitor is shown at the 2.5 σ contour level. Major hydrogen bonds are depicted with dashed lines, and distances are marked in Å.

Figure 8.
Active site structure of **14j** (**A**) (PDB 5FVW) or **14k** (**B**) (PDB 5FVX) bound to human nNOS. The omit $F_o - F_c$ electron density for the inhibitor is shown at the 2.5 σ contour level. Major hydrogen bonds are depicted with dashed lines, and distances are marked in Å. For comparison, panel (**C**) also shows active site structure of **5** (PDB 4UH5) bound to human nNOS.
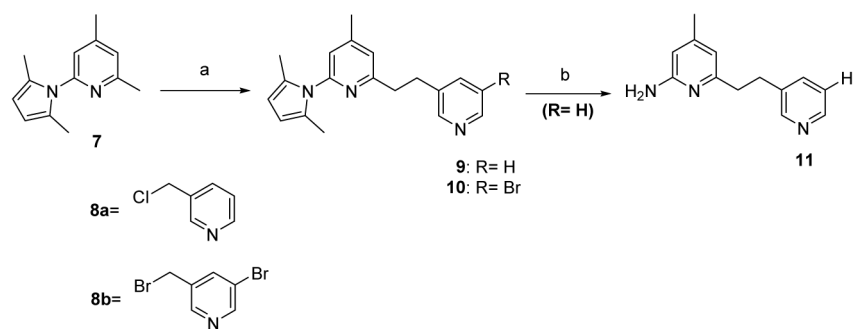
Scheme 1. Synthesis of intermediate 10 and compound 11

Reagents and conditions (a) **8a** or **8b**, *n*-BuLi, THF, −78 °C to 0 °C then −78 °C; (b) NH$_2$OH·HCl, EtOH/H$_2$O (2:1), 100 °C, 20 h.
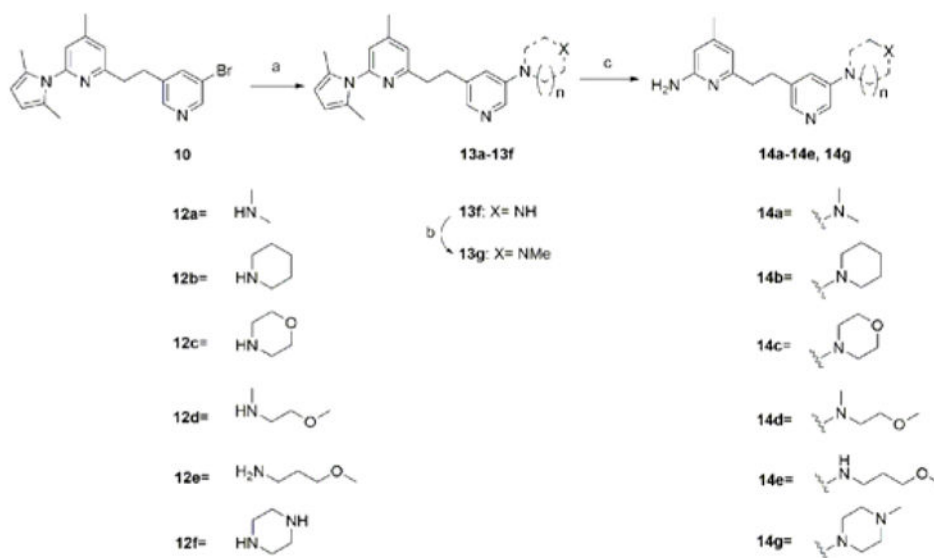
Scheme 2. Synthesis of compounds 14a-14e and 14g

Reagents and conditions: (a) **12a**, **12b**, **12c**, **12d**, **12e**, or **12f**, Pd$_2$(dba)$_3$, DavePhos, NaOt-Bu, dioxane, 100 °C, 20 h; (b) MeI, TEA, THF, r.t., 1 h; (c) NH$_2$OH·HCl, EtOH/H$_2$O (2:1), 100 °C, 20 h.
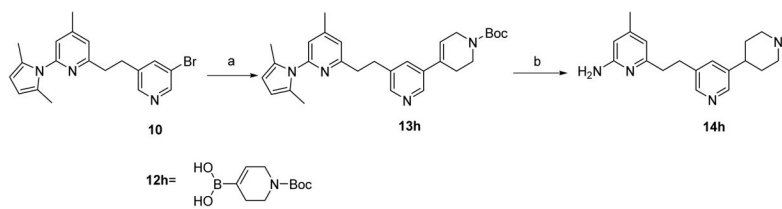
Scheme 3. Synthesis of 14h

Reagents and conditions (a) **12h**, Pd(OAc)$_2$, SPhos, K$_3$PO$_4$, Tol/H$_2$O (20:1), 100 °C, 20 h; (b) (i) Pd/C, H$_2$, MeOH, r.t., 20 h, (ii) LAH, THF, 0 °C to reflux, 1 h, (iii) NH$_2$OH·HCl, EtOH/H$_2$O (2:1), 100 °C, 20 h.
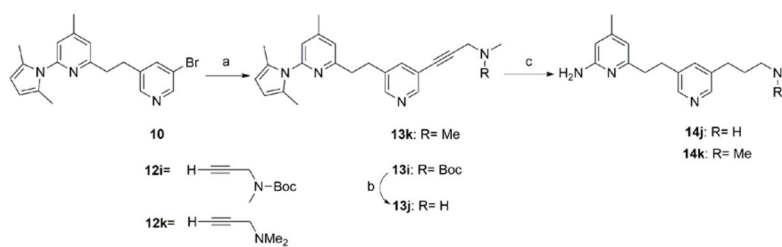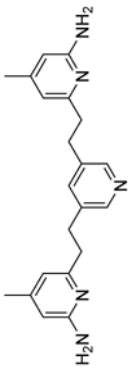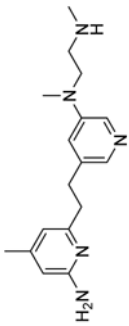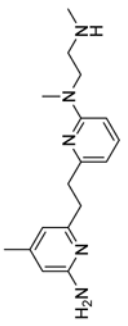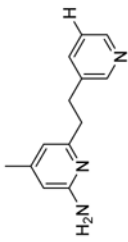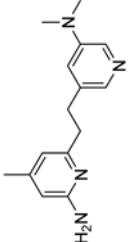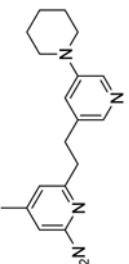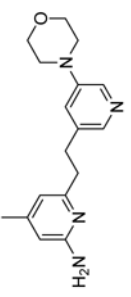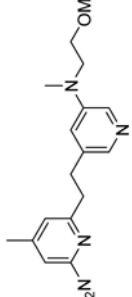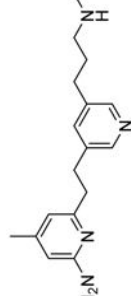
Scheme 4. Synthesis of compounds 14j and 14k

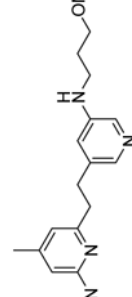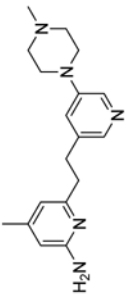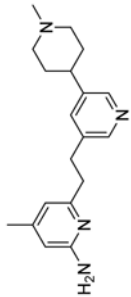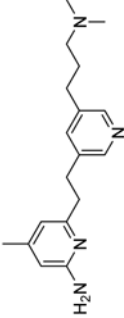Reagents and conditions: (a) **12i** or **12k**, Pd(PPh$_3$)$_4$, CuI, TEA, 90 °C, 20 h; (b) 20 % TFA in DCM, r.t., 1 h; (c) (i) Pd/C, H$_2$, MeOH, r.t., 20 h, (ii) NH$_2$OH·HCl, EtOH/H$_2$O (2:1), 100 °C, 20 h.

Table 1

Inhibition of non-human NOSs by 4-6, 11, 14a-14e, 14g-14h, 14j, and 14k

Cmpd	Structure	$K_i(nM)^a$			Selectivity^b	
		nNOS	iNOS	eNOS	n/i	n/e
4		25	1450	2680	58	107
5		17	2152	12910	127	759
6		35	4845	17742	138	507
11		706	2784	NT^c	4	NA^d
14a		139	1797	NT	13	NA
14b		1875	5642	NT	3	NA

Cmpd	Structure	K_i (nM)[a]			Selectivity[b]	
		nNOS	iNOS	eNOS	n/i	n/e
14c		547	11570	NT	21	NA
14d		1768	18233	NT	10	NA
14e		558	7053	NT	13	NA
14g		43	14214	> 30000	331	>698
14h		72	11779	20487	164	285
14j		16	1894	13247	118	828

Cmpd	Structure	$K_i(nM)^a$			Selectivity[b]	
		nNOS	iNOS	eNOS	n/i	n/e
14k		25	1486	16637	59	665

[a]K_i values are calculated directly from IC50 values. IC50 values are the average of at least two replicates from nine data points. All experimental standard error values are less than 15%.

[b]Selectivity values are determined by calculating the ratios of respective K_i values.

[c]NT = not tested

[d]NA = not applicable

Table 2

Inhibition of human nNOS by 5, 6, 14a, 14c, 14g, 14h, 14j, and 14k

Cmpd	K_i (nM)[a]		Selectivity[b]
	human nNOS	rat nNOS	human/rat
5	59	17	3.5
6	64	35	1.8
14a	425	139	3.1
14c	862	547	1.6
14g	84	43	2.0
14h	89	72	1.2
14j	13	16	0.8
14k	37	25	1.5

[a]K_i values are calculated directly from IC$_{50}$ values. IC$_{50}$ values are the average of at least two replicates from nine data points. All experimental standard error values are less than 15%

[b]Selectivity values are determined by calculating the ratios of respective K_i values.

Table 3

Inhibition of human eNOS by compounds 5, 6, 14a, 14c, 14g, 14h, 14j, and 14k

Cmpd	K_i (nM)[a]		Selectivity[b]
	human eNOS	human nNOS	n/e
5	5006	59	85
6	6621	64	103
14a	18271	425	43
14c	42563	862	49
14g	73006	84	869
14h	22536	89	253
14j	22895	13	1761
14k	39533	37	1068

[a] K_i values are calculated directly from IC_{50} values. IC_{50} values are the average of at least two replicates. All experimental standard error values are less than 15%.

[b] Selectivity values are determined by calculating the ratios of respective K_i values.

Table 4

Percent inhibition of selected cytochromes P450 isozymes by 14j

	(% inhibition)				(% inhibition)	
	Positive controls[a, b]	14j[a]			Positive controls[a, b]	14j[a]
CYP1A2	95	9	CYP2C19		89	11
CYP2B6	98	8	CYP2D6		93	6
CYP2C8	95	2	CYP3A4		100	58
CYP2C9	98	0				

[a]Performed at 10 μM concentration.

[b]Positive control inhibitors are: Fluvoxamine (CYP1A2), Ticlopidine (CYP2B6), Quercetin (CYP2C8), Sulfaphenazole (CYP2C9), Ticlopidine (CYP2C19), quinidine (CYP2D6), and ketoconazole (CYP3A4).